Applied and Environmental Microbiology, Dec. 2010, p. 7981–7989 Vol. 76, No. 24
0099-2240/10/$12.00 doi:10.1128/AEM.00650-10

Effects of Engineered Cerium Oxide Nanoparticles on Bacterial Growth and Viability▽†

Dale A. Pelletier,[1] Anil K. Suresh,[1] Gregory A. Holton,[1] Catherine K. McKeown,[1] Wei Wang,[2] Baohua Gu,[2] Ninell P. Mortensen,[1] David P. Allison,[1,3] David C. Joy,[4] Martin R. Allison,[1] Steven D. Brown,[1] Tommy J. Phelps,[1] and Mitchel J. Doktycz[1,4]*

Biosciences Division, Oak Ridge National Laboratory, Oak Ridge, Tennessee 37831-6445[1]; Environmental Sciences Division, Oak Ridge National Laboratory, Oak Ridge, Tennessee 37831-6422[2]; Department of Biochemistry & Cellular & Molecular Biology, University of Tennessee, Knoxville, Tennessee 37996-0840[3]; and Center for Nanophase Materials Sciences, Oak Ridge National Laboratory, Oak Ridge, Tennessee 37831-6488[4]

Received 15 March 2010/Accepted 5 October 2010

Interest in engineered nanostructures has risen in recent years due to their use in energy conservation strategies and biomedicine. To ensure prudent development and use of nanomaterials, the fate and effects of such engineered structures on the environment should be understood. Interactions of nanomaterials with environmental microorganisms are inevitable, but the general consequences of such interactions remain unclear, due to a lack of standard methods for assessing such interactions. Therefore, we have initiated a multianalytical approach to understand the interactions of synthesized nanoparticles with bacterial systems. These efforts are focused initially on cerium oxide nanoparticles and model bacteria in order to evaluate characterization procedures and the possible fate of such materials in the environment. The growth and viability of the Gram-negative species *Escherichia coli* and *Shewanella oneidensis*, a metal-reducing bacterium, and the Gram-positive species *Bacillus subtilis* were examined relative to cerium oxide particle size, growth media, pH, and dosage. A hydrothermal synthesis approach was used to prepare cerium oxide nanoparticles of defined sizes in order to eliminate complications originating from the use of organic solvents and surfactants. Bactericidal effects were determined from MIC and CFU measurements, disk diffusion tests, and live/dead assays. For *E. coli* and *B. subtilis*, clear strain- and size-dependent inhibition was observed, whereas *S. oneidensis* appeared to be unaffected by the particles. Transmission electron microscopy along with microarray-based transcriptional profiling was used to understand the response mechanism of the bacteria. Use of multiple analytical approaches adds confidence to toxicity assessments, while the use of different bacterial systems highlights the potential wide-ranging effects of nanomaterial interactions in the environment.

The physical and chemical properties of nanoparticles can vary significantly from those of their bulk counterparts. Unique properties, such as large surface area-to-volume ratios and the ability to selectively mediate chemical transformations, contribute to their usefulness as effective heterogeneous catalysts for fuel transformation, as novel probes for sensing and cell imaging, and as drug delivery agents. Nanoparticles associated with polymers, metal or metal oxides, liposomes, micelles, dendrimers, or metal sulfides are being considered for use in combating diseases such as cancer (12, 42) or fighting bacterial pathogens (30, 44, 46, 48). Beyond biomedical applications, there are established uses of nanoparticles for industrial applications and commercial products. Cerium oxide (CeO_2) nanoparticles are a prime example of a metal oxide nanomaterial with multiple industrial and biomedical uses. It is used extensively as an abrasive in semiconductor manufacturing, as a component in catalytic converters for automobile exhaust systems, as a fuel additive to promote combustion, as a UV light absorber, and as an electrolyte for fuel cells (24, 25). Recently, it has also been demonstrated that CeO_2 nanoparticles possess antioxidant activity at physiological pH values and therefore may be useful in biomedical applications for protecting cells against radiation damage, oxidative stress, or inflammation (38, 49a).

The same properties that make nanoparticles useful in a variety of applications can potentially make them toxic and harmful to the environment. The potential toxicity of nanomaterials has been recognized (4, 6, 20, 32, 49, 51), and reviews and perspectives are available (3, 16, 23, 32, 34). Nevertheless, a better understanding of the risks associated with specific nanomaterials may reduce environmental damage or adverse health effects (15, 22). While little is known about the environmental fate, transport, and accumulation of CeO_2 nanoparticles, they are produced at industrial scales for use as a diesel fuel additive (typically at a concentration 5 mg/liter) and as a polishing agent (35, 37). The emergence of multiple, important applications for CeO_2 nanoparticles and increased industrial production will undoubtedly lead to environmental release of nanoparticles and has prompted increased research into their properties and potential toxicity to biological systems. Various efforts have led to seemingly different assessments. Park et al. described CeO_2 nanoparticles inducing oxidative stress in human lung epithelial cells (27). In contrast, Schubert et al. reported that CeO_2 nanoparticles act as antioxidants and protect

* Corresponding author. Mailing address: Biosciences Division, Oak Ridge National Laboratory, Bethel Valley Road, Oak Ridge, TN 37831-6445. Phone: (865) 574-6204. Fax: (865) 574-5345. E-mail: doktyczmj@ornl.gov.

† Supplemental material for this article may be found at http://aem.asm.org/.

▽ Published ahead of print on 15 October 2010.

cells from oxidative damage (43). Recent findings also suggest that pH and other factors may determine whether CeO_2 nanoparticles destroy or help cells (2). Further complicating toxicity interpretations are the effects of the synthesis methodology; various manufacturing processes may incorporate additives, detergents, and solvent chemicals that are not completely removed from the final product. For example, C_{60} was initially deemed to be toxic, but later studies indicated that remnants of tetrahydrofuran (THF) used in the synthesis of C_{60} were responsible for the toxicity (18). Thus, the apparent biological properties of nanomaterials may depend in part on other constituents present in the formulation. Commercial sources of nanoparticles often do not provide information regarding synthesis methods or the use of stabilizing/capping agents. Consequently, the findings of studies assessing the toxicity of nanoparticle suspensions may be difficult to interpret.

To date, the majority of studies regarding toxicity evaluations of metal oxide nanoparticles have involved the use of mammalian cells. Relatively fewer studies have focused on the effects of CeO_2 and other metal oxide nanoparticles on bacterial systems (20). Thill et al. reported that commercial CeO_2 nanoparticles were toxic to *Escherichia coli* in KNO_3 solution due to an oxidative reaction when the nanoparticles adsorbed to the bacterial cell surface (51). In contrast, investigations by other researchers concluded that there was no apparent bacterial toxicity due to CeO_2 nanoparticles (26, 52). Differences in reported toxicity can be ascribed to many factors. These can include the origin of the materials used for their synthesis, the presence of stabilizing or capping agents, the chemical and physical properties of the nanoparticles, as well as the procedures employed to evaluate toxicity and can make it difficult to form conclusions. Therefore, the present investigation aims to evaluate different approaches appropriate for assessing bacterial toxicity using well-characterized materials and standard bacterial assay systems. Specifically, this study examines the effects of nanoparticle concentration, particle size, exposure time, growth medium, and pH on the growth and viability of *E. coli*, *Bacillus subtilis*, and *Shewanella oneidensis*. Additionally, studies that potentially reveal nanoparticle-bacterium interaction mechanisms are described.

MATERIALS AND METHODS

All bacterial strains used were wild-type strains purchased from the American Type Culture Collection, Manassas, VA (BD Biosciences, Franklin Lakes, NJ), namely, *Escherichia coli* (ATCC 700926), *Bacillus subtilis* (ATCC 6633), and *Shewanella oneidensis* (MR-1). All other chemicals used were of reagent grade and were from standard commercial sources.

Synthesis of cerium oxide nanoparticles. CeO_2 nanoparticles were synthesized through a modified surfactant and template-free synthetic route as described earlier (53) (see the supplemental material for details).

Physical characterization. UV-visible light absorbance measurements were recorded on a Cary 100 Bio spectrophotometer (Varian Instruments, CA) operated at a resolution of 1 nm. Dynamic light-scattering (DLS) and zeta potential measurements were performed on a 90 Plus/BI-MAS particle size analyzer (Brookhaven Instruments Corp., NY). For all experiments the nanoparticle suspensions were dispersed in Milli-Q water and sonicated for 5 min in a water bath sonicator at 40 kHz (model 2510; Branson Ultrasonic Corporation, CT). DLS was used to determine the hydrodynamic sizes and the point of zero charge (pzc) of the nanoparticle suspensions. The pzc is defined as the point where the electrical charge density on the surface of the nanoparticles is zero. Raman spectroscopy for the dried nanoparticle powder was performed on a Renishaw Raman spectrometer equipped with a Leica microscope and a 785-nm diode laser at a spectral resolution of $\sim$2 cm^{-1} and a laser power of 20 mW. X-ray diffraction (XRD) measurements were performed on a Discover D8 X-ray diffractometer with a Xe/Ar gas-filled Hi-Star area detector and an *xyz* platform, operated at 40 kV and at a current of 40 mA. Transmission electron microscopy (TEM) measurements of nanoparticle samples drop coated on carbon-coated copper grids were imaged on a Hitachi HD-2000 scanning transmission electron microscope (STEM) operated at an acceleration voltage of 200 kV. TEM for the nanoparticle-treated bacteria was carried out by placing a 5-μl droplet on the grid, incubating for 7 min, rinsing by plunging the grid into Milli-Q water, and air drying prior to imaging. For atomic force microscopy (AFM), 5-μl samples were prepared from 1,000-fold dilutions of a 0.5% (wt/vol) nanoparticle stock in Milli-Q water, placed on freshly cleaved mica surface, and spread with a micropipette tip. AFM measurements were collected in air in contact mode with a PicoPlus atomic force microscope (Agilent Technologies, Tempe, AZ) using a 10-μm scanning head at 512 pixels per line scan and a scan speed of 1 line/s. The cantilevers used were Veeco silicon nitride probes (MLCT-AUHW; Veeco, Santa Barbara, CA).

Bacteriological toxicity assessment. (i) Disk diffusion tests. Bacterial sensitivity to different-sized CeO_2 nanomaterials was tested by disk diffusion tests as described by Ruparelia et al. (41). Small Whatman filter paper disks of uniform size (diameter, 6 mm) were placed separately in each of the four prepared 0.5% (wt/vol) CeO_2 nanoparticle suspensions for 5 min; the disks were carefully removed using sterile forceps. After the bacterial suspension (100 μl of 10^4 to 10^5 CFU ml^{-1}) was uniformly plated on LB agar plates, a disk containing nanoparticles was placed at the center of each plate and the plate was incubated at 37°C for 18 h. The average diameter of the inhibition zone (DIZ) surrounding the disks was measured to determine inhibition.

(ii) Determination of MIC. The MIC, defined as the lowest concentration of a compound that inhibits the growth of an organism (39), was determined for *E. coli* in LB medium at pH 7.2 and in M9 minimal medium (21) at pH 6.4, 7.2, and 7.8. *B. subtilis* was tested in LB and minimal media (47) at pH 7.2, and *S. oneidensis* was tested in LB and HBA minimal media (13) at pH 7.2. Reactions were carried out in test tubes containing 5 ml of the logarithmic-phase ($\sim$0.098) bacterial cultures and different-sized CeO_2 nanoparticles at various concentrations (50, 100, and 150 mg/liter). Tubes with sterile media containing no nanoparticles or nanoparticles only served as controls. Samples were incubated on a shaker (200 rpm) at 37°C (*E. coli* and *B. subtilis*) or 30°C (*S. oneidensis*), with growth monitored by obtaining measurements of the optical density at 600 nm (OD_{600}) every 30 min for 8 h.

(iii) CFU measurements. Studies of *E. coli* and *B. subtilis* viability were performed in liquid cultures at a nanoparticle concentration of 100 mg/liter. Aliquots were taken at 0, 1, 5, and 24 h and serially diluted in the appropriate minimal medium, and the dilutions were plated on LB agar plates. After overnight incubation at 37°C, the numbers of CFU were counted manually.

(iv) Live/dead viability assay. *E. coli* and *B. subtilis* cultures grown to logarithmic phase in M9 medium and *B. subtilis* minimal medium, respectively, were treated with different concentrations (50, 100, and 150 mg/liter) of CeO_2 nanoparticles. Following exposure, the impact on bacterial membrane integrity was assessed using a live/dead BacLight bacterial viability kit (Invitrogen) as instructed by the manufacturer. To quantify the relative numbers of live and dead cells, the relative fluorescence intensities were measured using a fluorescence plate reader (excitation at 485 nm, emission at 525 and 625 nm).

(v) Monitoring superoxide production. Superoxide production upon exposure of bacterial suspensions to various concentrations of CeO_2 nanoparticles was monitored by following the absorbance at 470 nm due to the reduction of 100 μM 2,3-bis(2-methoxy-4-nitro-5-sulfophenyl)-2*H*-tetrazolium-5-carboxanilide (XTT) to XTT-formazan by superoxide (O_2^-) (11, 29).

(vi) Microarray hybridization and analysis. For microarray experiments, an overnight *E. coli* culture was used to inoculate 250-ml flasks containing 100 ml of prewarmed M9 medium to an OD_{600} of $\sim$0.1 and incubated at 37°C with shaking at 200 rpm until mid-log phase (OD_{600}, $\sim$ 0.5). Cultures were treated with either prewarmed CeO_2 nanoparticles (100 mg/liter), cerium chloride (50 mg/liter), or Milli-Q water. After 1 h, cells were harvested by rapid centrifugation (5,000 $\times$ *g*, 2 min at 4°C) and snap-freezing in liquid N_2. Three separate controls and three experimental cultures were examined for each condition. Total cellular RNA was isolated as described earlier (8), except that the cells were first resuspended in TE (Tris-EDTA) buffer and incubated with 1 mg/ml of lysozyme to lyse the cells. Purified, fluorescently labeled cDNA was hybridized to *E. coli* K-12 gene expression 4-by-72 K arrays (Roche NimbleGen, Madison, WI) using a Nimblegen hybridization system (BioMicro Systems, Inc., Salt Lake City, UT), according to the manufacturer's instructions. Microarrays were washed according to the array manufacturer's procedure. Briefly, microarray mixers were removed in 42°C Nimblegen wash buffer I and then washed manually in room temperature buffers: wash buffer I for 2 min, wash buffer II for 1 min, and wash buffer III for 15 s.

TABLE 1. Average dimensions of the different cerium oxide nanoparticles measured by DLS, TEM (long and short axes), and AFM (long axis and height)

Sample	Avg particle size (nm)[a]				
	DLS	TEM		AFM	
		Long axis	Short axis	Height	Long axis
A	28.9 ± 18.4	6 ± 3.5		2.02 ± 0.58	
B	38.1 ± 14.1	15 ± 4.3	9 ± 4.2	11.64 ± 3.85	129.04 ± 36.83
C	65.7 ± 15.2	22.3 ± 5.7	14 ± 2.9	12.43 ± 4.11	138.67 ± 39.01
D	126.8 ± 24.1	45 ± 5	25 ± 11	28.04 ± 17.24	175.27 ± 57.47

[a] For dynamic light scattering measurements, average particle sizes were determined from three separate experiments. For TEM and AFM measurements, average particle sizes were determined by counting ~100 particles from more than three different images.

Microarrays were dried for 80 s using a Maui wash system (BioMicro Systems, Inc.) and then scanned with a Surescan high-resolution DNA microarray scanner (Agilent Technologies, Santa Clara, CA), and the images were quantified using Nimblescan software. Raw microarray data were $\log_2$ transformed and imported into the statistical analysis software JMP Genomics (version 4.0; SAS Institute, Cary, NC) as described previously (54). Microarray data were normalized using the Lowess normalization algorithm within JMP Genomics, and an analysis of variance (ANOVA) was performed to determine significant differences in gene expression levels between conditions and time points using the false discovery rate testing method ($P < 0.01$).

RESULTS AND DISCUSSION

Synthesis and characterization of CeO_2 nanoparticles. CeO_2 nanoparticles of various sizes were synthesized and characterized in terms of their morphologies, dimensions, and surface charges. A hydrothermal synthesis approach was used (53). This approach enables the synthesis of nanoparticles of different sizes without changing the reagent set or using detergents and organic solvents that could potentially interfere with toxicity assessments. Batches of CeO_2 nanoparticles with nominal sizes of 6 ± 3.5, 15 ± 4.3, 22 ± 5.7, and 40 ± 10 nm (as measured by electron microscopy) were prepared, in order to assess potential size-dependent interactions with bacteria, and were designated samples A, B, C and D, respectively.

Accurate sizing of the nanoparticles was determined using a range of techniques, including DLS, TEM, and AFM. The results are summarized in Table 1 and varied depending on the technique used. By TEM, the average length of the long and short axes of the particles increases from samples A to D (Fig. 1). The standard deviation in size distribution is fairly consistent, and each sample contains a distinct range of particle sizes, as illustrated by the histogram (see Fig. S1 in the supplemental material). The smallest particles (sample A) were more or less square shaped, with a few ovoid particles (Fig. 1a and e). The B sample contains a preponderance of circular and ovoid shapes. Additionally, edges are often apparent on the ovoid particles and a few cuboidal particles are evident (Fig. 1b). The C sample contains ovoid along with rectangular and triangular particles (Fig. 1c). AFM deflection images of these particles begin to reveal multiple-step edges in the particles that may be breaks in the crystal planes or simply clumps of particles (Fig. 1g). Also, single particles appear to have long and short axes consistent with the TEM images. Sample D, containing the

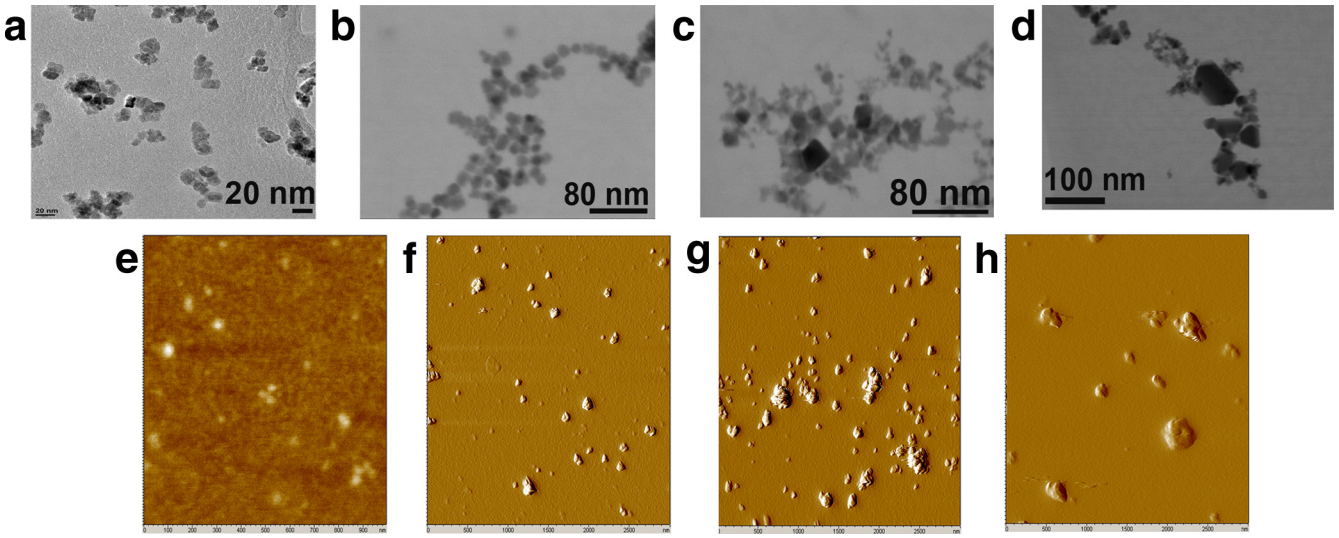

FIG. 1. TEM and AFM analyses of the four different sizes of cerium oxide nanoparticles. (a to d) TEM images of the smallest to the largest CeO_2 particles, referred to as samples A (a), B (b), C (c), and D (d). (e to h) AFM images of the particles; (e) sample A and its topographic image that is used to accurately measure height; (f to h) deflection images of the sample B, C, and D particles, respectively. The deflection images better represent changes in surface morphology of the CeO_2 nanoparticles.

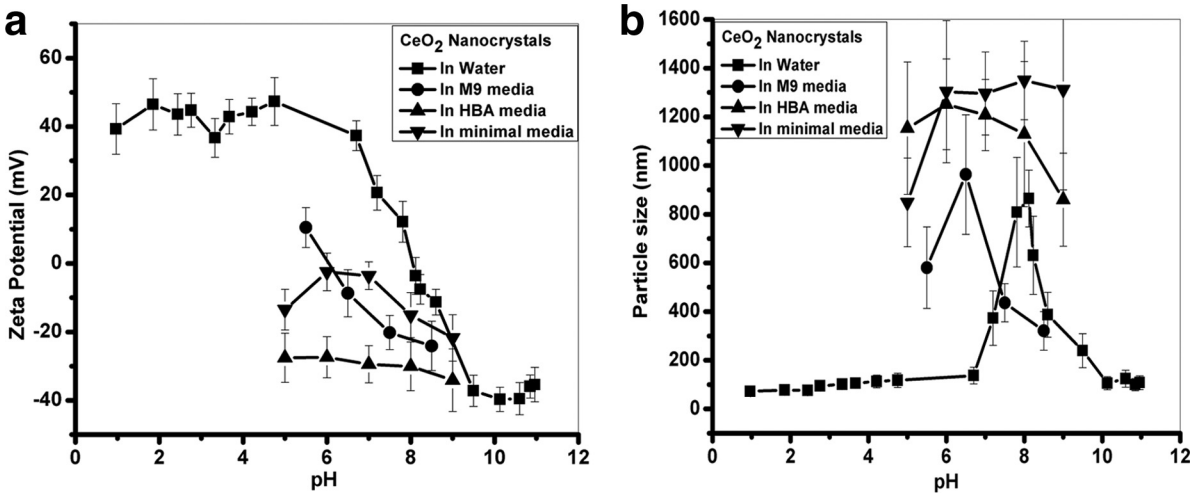

FIG. 2. Zeta potential and dynamic light scattering measurements of the B sample of cerium oxide nanoparticles. The zeta potential (a) and hydrodynamic sizes (b) of the B sample of cerium oxide nanoparticles in water and M9, *B. subtilis* minimal, and HBA media under different pH conditions are shown. Similar results were obtained with the other nanoparticle samples.

largest particles, continues this trend and displays a variety of different particle shapes (Fig. 1d). AFM topographic images also show a range of heights among the four particle preparations. The size distribution values obtained by AFM differed significantly from the TEM data, which can be partially attributed to complications due to the scanning probe tip. Height measurements by AFM can be accurate, while lateral measures can be difficult to determine accurately due to convolution by the scanning probe tip; however, relative differences in length can be resolved by using the same probe tip. Between the different sample sets, differences in the length measurements of the long axes are slightly larger than the differences between the values obtained by TEM. These differences are likely attributed to difficulties in clearly assigning particle edges by either technique. Nevertheless, AFM-based height measurements of the different samples are consistently less than the long-axis measurements observed by TEM. Height measurements are difficult to obtain from TEM images. Therefore, from the combined AFM and TEM analyses, we conclude that the majority of particles in samples A, B, and C range from spherical to flattened square and ovoid or capsular structures, while sample D consists of larger crystals with greater shape heterogeneity.

The particles appeared much larger by dynamic light scattering than by TEM and AFM (Table 1). This size difference can be attributed to particle clumping in the DLS data, while EM and AFM allow latitude for eliminating clumps of particles from the analysis. The EM images (Fig. 1) showed crystalline particles, which are also confirmed by X-ray diffraction data (see Fig. S2a in the supplemental material) and are consistent with the reported peaks of pure CeO_2 (14). Further, Raman spectroscopy measurements (see Fig. S2b in the supplemental material) agree well with literature values for pure CeO_2 nanoparticles (36).

The CeO_2 nanocrystals were further investigated for surface charge, hydrodynamic size, and size distributions under various pH conditions using DLS. The CeO_2 nanocrystals exhibit a pzc at pH 8.0 (Fig. 2a), which is consistent with reported values of pH 8.1 (10), implying that they are positively charged under acidic and neutral pH conditions (pH $<$ 8.0) but become negatively charged at pH values above 8.0. Our results suggest that the pzc for the four samples of nanocrystals is not size dependent. The pzc shifted to a lower pH value (at a pH of ~6) in the M9 minimal medium used for the *E. coli* growth studies and can be attributed to the adsorption of anions in the relatively-high-ionic-strength solution.

The stability of the CeO_2 nanocrystals was studied in water and the different minimal media used for bacterial growth, as aggregation behavior can potentially affect nanoparticle-bacterium interactions and therefore toxicity. As expected, at pH values near the pzc, the nanocrystals aggregated, as revealed by an increase in hydrodynamic size ($>$500 nm) in all the different media tested (Fig. 2b). The hydrodynamic sizes of all four samples of nanocrystals increased as the pH increased up to ~8 in water and decreased at higher pH values due to surface charge reversal. In M9, HBA, and *B. subtilis* minimal media, the aggregation was greater near the pzc (pH 6), and even at pH 7.5 and 8.5, the measured hydrodynamic size was $>$300 nm (see Fig. S3 in the supplemental material). The tendency of small particles to aggregate in a given medium depends on properties such as particle concentration and composition of the medium, including ionic strength and salt concentration (17, 31).

Overall, the physical characterizations of the different CeO_2 nanoparticles indicated heterogeneities and chemical properties associated with the samples that may need to be accounted for when toxicity data are interpreted. Clearly, even with refined synthesis procedures, a range of physical structures is present. These structures may have different biological reactivities that can complicate interpretations. Further, the pzc of the particles is near neutral pH values and can cause the particles to agglomerate at pH values optimal for bacterial growth. This pzc can also shift in the different media used for bacterial growth, indicating the presence of other medium components competing for particle binding sites.

Bacterial growth and viability measurements upon exposure to CeO_2 nanoparticles. The potential antibacterial activity of the CeO_2 nanoparticles was investigated using *E. coli*, *S. oneidensis*, and *B. subtilis* and several measures of bacterial growth and viability to evaluate their utility. DIZ, MIC, live/dead staining, and CFU assays were performed.

For the three bacterial species that were evaluated, the observed growth inhibition trends were similar for all assays performed (Fig. 3; see Fig. S4 in the supplemental material). Further, in cases where growth inhibition occurred, bacterial growth rates depended on nanoparticle concentrations in the range of 50 to 150 mg/liter. It should be noted that the DIZ assay is prone to artifacts arising from factors such as the diffusion rate, particle adsorption to the disk, and the hydrophobic/hydrophilic nature of the particle. Nevertheless, the live/dead staining assay results and the CFU measurements agreed qualitatively with the trends observed by the disk diffusion assay (see Fig. S4 in the supplemental material). While the overall trends between assays were similar, differential effects between test organisms were observed. For *S. oneidensis*, none of the nanoparticle samples showed growth inhibition (data not shown). In contrast to *E. coli* and *B. subtilis*, *S. oneidensis* incorporates metal reduction into its metabolism and may in general be more resistant (5) to metal oxide nanoparticles than *E. coli* and *B. subtilis*. With *E. coli*, growth inhibition decreased as the sample size increased for samples B, C, and D, while the smallest particles had little affect (Fig. 3). The reverse trend was observed for *B. subtilis*. The sample B particles had no significant affect on the organism, while the sample A, C, and D particles exhibited inhibitory growth effects (Fig. 3).

To further investigate this difference in the antibacterial potential of the various CeO_2 nanoparticles, MIC assays were carried out for *E. coli*, *S. oneidensis*, and *B. subtilis* in complex or minimal media. In LB medium, neither *E. coli* nor *B. subtilis* was inhibited during log-phase growth for any concentration or size of nanoparticle (data not shown), in agreement with the results from Thill et al., who suggested that interactions between the nanoparticles and the organic material in the LB medium render the nanoparticles inert to *E. coli* (51). However, some samples of the particles inhibited growth of *E. coli* and *B. subtilis* in minimal medium, with inhibition being concentration dependent (Fig. 3b to e).

The differences in the reactivities of the nanoparticles to the bacteria may be a result of the morphology of these particles or the greater ratio of surface area to mass that occurs as particle size decreases. The smaller particles tend to agglomerate to a greater extent, which may lead to different binding characteristics. Also, particles with uneven and rough surfaces or with irregular shapes have corners and edges that can be biologically and chemically reactive. Atoms at these locations have a lower bonding coordination (weaker bonds) than bulk atoms and therefore bind to foreign molecules more efficiently (40, 50).

Another origin for differences in reactivity can be the medium. For example, the medium pH can alter nanoparticle surface charge and thus adsorption affinity of the particles toward the bacteria. However, changes in the medium pH across the range of 6.9 to 7.8 did not alter the effects of the nanoparticles on bacterial growth (data not shown). Although pH can alter the surface charge of the CeO_2 nanoparticles and potentially the adsorption affinity of the nanoparticles toward the bacteria (2), the buffering range of the minimal medium and the inability of the bacteria to grow at extreme pH ranges limited experimental evaluations. Above pH 7.8, elements in M9 medium began to precipitate, and at pH values below 6.4, the medium lost its buffering capacity.

Certainly, other factors besides nanoparticle size, such as surface area, bioavailability, particle aggregation, structural distortion, and growth medium can impact nanoparticle inhibition/toxicity. Others have also observed a difference between *E. coli* and *B. subtilis* in their reactivities to nanoparticles. When the toxicities of TiO_2, SiO_2, and ZnO particles on *E. coli* and *B. subtilis* were compared, greater antibacterial activity toward *B. subtilis* than toward *E. coli* was observed (1). While the mechanistic bases for differences in reactivity between *E. coli* and *B. subtilis* are still obscure, one could hypothesize that these differences are due to (i) differences in membrane surfaces, (ii) metabolic differences, and (iii) potential effects on spore formation in the case of *B. subtilis*. However, no differences in *B. subtilis* sporulation were observed upon microscopic examination of cells with or without nanoparticle exposure. Clearly, bacterial interactions with nanoparticles can vary across a spectrum of responses, requiring a better understanding of the molecular mechanisms involved. However, the multiple measures of bacterial growth and viability in the presence of the different sizes of CeO_2 nanoparticles reveal both consistent and conflicting trends that caution the application of general conclusions regarding bacterium-nanoparticle interactions. It appears that the presence of CeO_2 nanocrystals can inhibit the growth of some bacteria, but the material is not necessarily bactericidal and the growth of both *E. coli* and *B. subtilis* was inhibited in a concentration-dependent manner.

Mechanistic investigations of bacterium-CeO_2 interactions. Imaging experiments and molecular analyses were performed to evaluate the molecular mechanisms that underlie the bacterial response to the CeO_2 nanoparticles. These assessments focused on the effects of the B sample of the CeO_2 nanoparticles on *E. coli* due to its demonstrated inhibition of cell growth. An analysis of the molecular mechanisms can ultimately be used to classify bacterial response mechanisms. To assess direct interactions between the sample B CeO_2 nanoparticles and *E. coli* grown in M9 medium, STEM imaging experiments were performed (Fig. 4), and the findings suggest that the nanoparticles adsorb to but do not penetrate the bacterial cells. Additionally, clusters of particles are seen, consistent with the light scattering-based characterizations (Fig. 2b). The imaging results also agreed with those reported by Thill et al., who suggested that the adsorption of nanoparticles to the bacterial cell walls accounts for their deleterious effects (51).

For elucidation of potential molecular mechanisms, two basic approaches were investigated: a directed approach that assessed putative response mechanisms and a discovery-based approach that employed microarray technology to identify the genetic response of *E. coli* to the nanomaterial. Reactive oxygen species generation has been implicated in the toxic response of a number of biological systems to nanoparticles (11, 29). The presence of superoxide was examined using an XTT assay, which yields a colorimetric signal when XTT is reduced

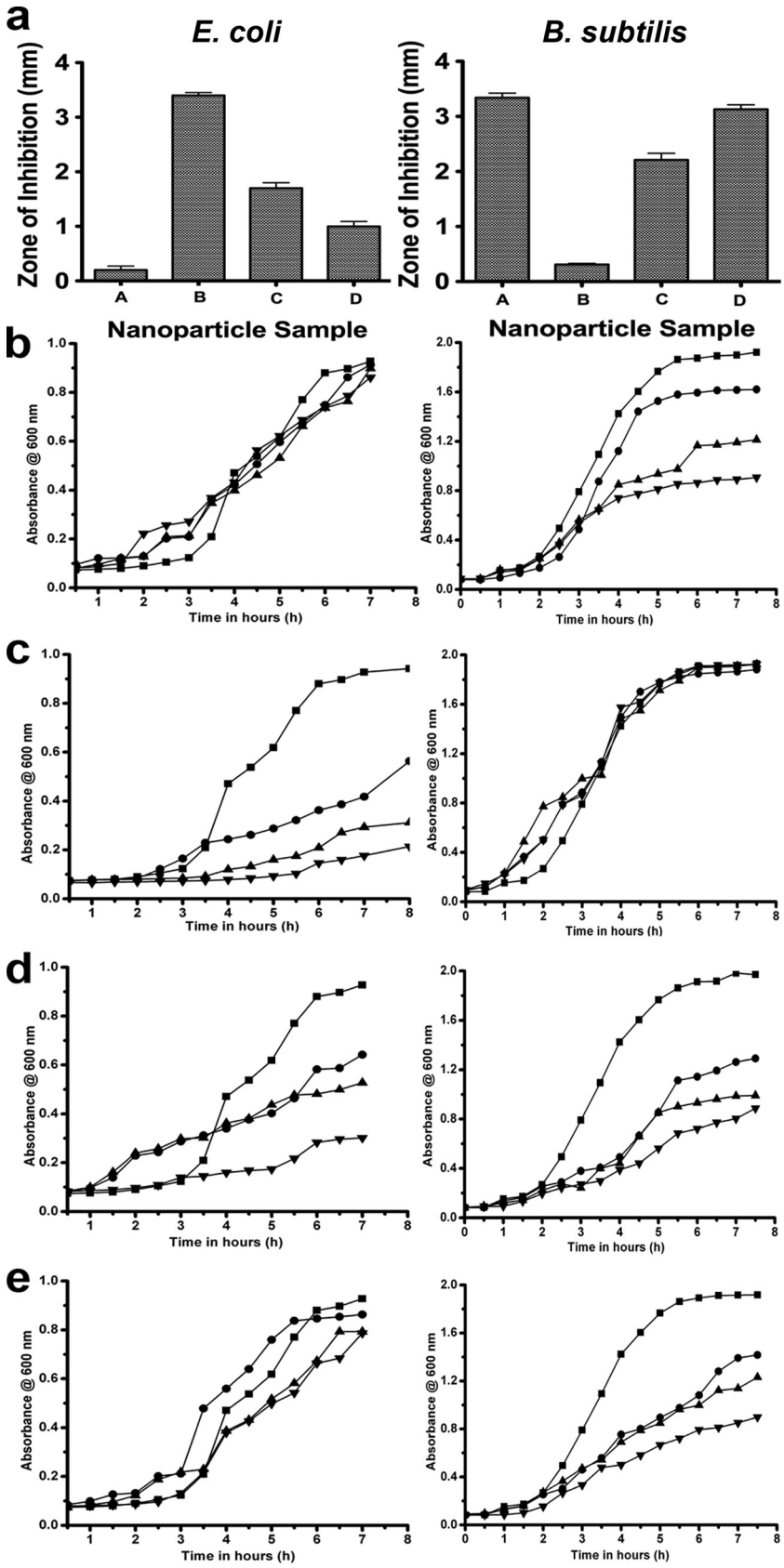

FIG. 3. Diameter of zone of inhibition and MIC assays for *E. coli* and *B. subtilis* induced by different-sized sample A, B, C, and D cerium oxide nanoparticles. (a) Measurement of the diameter of the zone of inhibition (in millimeters) was carried out by disk diffusion assay, and the results are shown in the form of bar graphs for *E. coli* (left panel) and *B. subtilis* (right panel). (b to e) Dynamic growth curves for *E. coli* (left panels) and *B. subtilis* (right panels) in their respective minimal media treated with different sized cerium oxide nanoparticles at various concentrations (■, cells alone; ●, 50 mg/liter; ▲, 100 mg/liter; ▼, 150 mg/liter). (b) sample a; (c) sample B; (d) sample C; (e) sample D.

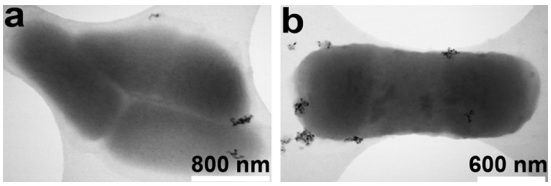

FIG. 4. Representative TEM images showing the interaction of *E. coli* and the B sample of cerium oxide nanoparticles at different magnifications. The images shows the results of incubating nanoparticles with logarithmic-phase growing bacteria for 30 min at 37°C with shaking, followed by placing a droplet on the EM grid for 7 min, rinsing in water to remove unbound bacteria and particles, and imaging. Particles apparently stick to the bacterial surfaces but are not internalized by *E. coli.*

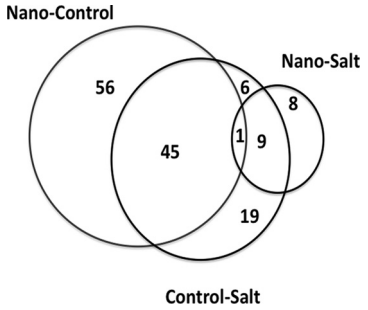

FIG. 5. Proportional Venn diagram analysis of significant differentially expressed genes. Nano-Control, sample B CeO_2 nanoparticle–Milli-Q control differences; Nano-Salt, sample B CeO_2 nanoparticle–$CeCl_3$ control differences; Conrol-Salt, Milli-Q control–$CeCl_3$ control differences. For a complete list of genes within categories A to G, see Table S1 in the supplemental material.

by superoxides. However, assays involving either *E. coli* or *B. subtilis* yielded negative results (see Fig. S5 in the supplemental material). A range of apparently contradictory responses from oxidative stress (27) to antioxidant and protective responses (43) has been described for CeO_2 nanoparticles in different systems. The origins of these differences are difficult to ascertain, but they do highlight the need for well-characterized nanoparticles and well-controlled studies.

Growth and viability assays involving cerium chloride and *E. coli* were also evaluated. A clear concentration-dependent response was observed between 25 and 150 mg/liter of $CeCl_3$ (see Fig. S6 in the supplemental material). A growth-inhibitory effect that is not lethal has been observed previously (20). Ingram examined the effects of salts, including $CeCl_3$, on *B. subtilis* respiration rates and concluded that the inhibition of respiration was likely due to the cations, not anions. He suggested that $CeCl_3$ was a more potent inhibitor than inhibitors of mono- or divalent metals (19). Sobek and Talburt found cerium [as $Ce(NO_3)_3$] bound rapidly to *E. coli* and altered the cellular composition of protein and lipid fractions compared to their compositions in untreated and $NaNO_3$-treated cells (45). They demonstrated oxygen uptake inhibition in $Ce(NO_3)_3$-treated cells.

For discovery of genetics-based response mechanisms, the global transcriptomics of *E. coli* after exposure to CeO_2 nanoparticles was assessed using whole-genome microarray analysis, and the results were compared to those of treatments with cerium chloride or water. In the microarray experiments, there was only a slight impact on cell growth and no appreciable differences in culture responses to the respective treatments (see Fig. S7 in the supplemental material). Overall, 144 genes were identified to be differentially expressed at statistically significant values [$-\log_{10}(P) > 3.8$] in an ANOVA model using a stringent false discovery rate testing method ($\alpha = 0.01$). Of these genes, 62 showed 2-fold or greater differences in relative gene expression for all the pairwise comparisons (Fig. 5; see Table S1 in the supplemental material).

Further analysis of the microarray data indicated that the cells treated with CeO_2 nanoparticles or $CeCl_3$ had higher levels of *cydAB* transcripts than the controls (Table 2). The expression of *cydAB* is known to be induced by iron limitation (9) and oxidative stress exposure (28). The increased abundance in transcripts encoding NirD and the high-affinity terminal oxidase cytochrome *bd-I* used under microoxic conditions, with the concomitant low levels of expression for the succinate dehydrogenase and cytochrome *b* terminal oxidase genes, was indicative of cerium (in either nanoparticle or ionic form) disrupting *E. coli* respiration, iron limitation, or oxidative stress (Table 2). Consistent with the interpretation of the cerium salt exposure data (45), the presence of cerium alters electron flow and respiration of *E. coli* (Table 2). The *groES* and *sodA* genes showed higher expression levels following treatment with water than with either of the other two treatments, indicating that the latter two treatments did not elicit major oxidative stress responses under the conditions used in this study. This observation is in agreement with the results of the XTT assays, which showed no detectable superoxide.

A proportional Venn diagram analysis (Fig. 5) showed that many of the iron uptake genes responded significantly in the nanoparticle treatment compared to the water treatment, while the *cus* operon responded significantly in both the CeO_2 nanoparticle and salt treatments compared to the control treatment. There was no significant differential gene expression from these loci when the CeO_2 nanoparticle and salt treatments were compared (see Table S1 in the supplemental material). Eight genes (*rnt*, *thiS*, *cysW*, *yciW*, *cysI*, *ilvG*, *cysN*, *pyrB*) were significantly differentially expressed between the CeO_2 nanoparticle and salt treatments (Fig. 5). The majority of these genes are involved in sulfur metabolism and, like other related genes, such as *cysD* and *cysJ*, responded to other treatments. A number of previous studies have shown relationships between genes involved in sulfur metabolic processes, iron uptake, respiration, and different stress responses (7, 8, 55). Collectively, the transcriptomic results of the present study are indicative of a mild, general stress response and a highly interrelated, complex, and coordinated gene regulatory network response.

Conclusion. The increasing use of nanoparticle-based products emphasizes the need to understand interactions between these materials and living systems and the need to standardize methods for toxicity assessments. The present investigation examined the potential toxicity of engineered cerium oxide nanoparticles in relation to their size on different bacteria. The importance of using well-characterized nanomaterials of a known synthesis route has been highlighted. Cerium oxide nanoparticles showed growth inhibition toward *E. coli* and *B.*

TABLE 2. Differential gene expression for selected respiratory genes

Gene	Product	Relative gene expression difference (fold change) for pairwise comparisons[a]		
		Nano/con	Nano/salt	Salt/con
cyoA	Cytochrome *o* ubiquinol oxidase subunit II	**0.5 (6.5)**	1.0 (0.1)	**0.5 (6.3)**
sdhC	Succinate dehydrogenase cytochrome b_{556} large membrane subunit	**0.5 (11.4)**	1.4 (3.2)	**0.4 (19.1)**
sdhD	Succinate dehydrogenase cytochrome b_{556} small membrane subunit	**0.4 (6.9)**	1.5 (1.4)	**0.3 (10.7)**
sdhA	Succinate dehydrogenase flavoprotein subunit	**0.5 (11.6)**	1.3 (1.5)	**0.4 (15.7)**
sdhB	Succinate dehydrogenase, fes subunit	**0.5 (4.3)**	1.2 (0.6)	**0.4 (5.9)**
cydA	Cytochrome *d* terminal oxidase, subunit I	**1.9 (7.5)**	1.0 (0.2)	**2.0 (7.4)**
cydB	Cytochrome *d* terminal oxidase, subunit II	**2.0 (9.8)**	0.9 (0.2)	**2.2 (10)**
nirD	Nitrite reductase small subunit	**1.8 (5.5)**	1.1 (0.4)	1.6 (3.5)

[a] Relative gene expression differences are presented as the arithmetic mean ratios derived from fluorescence intensities for each pairwise comparison. Nano/con, CeO_2 nanoparticle/Milli-Q control; Nano/salt, CeO_2 nanoparticle/$CeCl_3$ control; Salt/con, $CeCl_3$ control/Milli-Q control. Each expression difference considered significant is shown in boldface, and *P* values are presented in parentheses as $-\log_{10}$ values.

subtilis in minimal medium as a function of the nanoparticle size. The observed size-dependent response may result from size-dependent characteristics of the cerium oxide nanoparticles and/or metabolic characteristics of the different organisms. However, the role of the different media used to grow these bacteria and the interactions of the nanoparticles with these media must be considered when a bacterial response is assessed. In contrast, *S. oneidensis* growth was not inhibited by the cerium oxide nanoparticles. Collectively, these results suggest that nanoparticle interactions with bacteria can vary. Redundant measures of bacterial growth and toxicity in the presence of the different materials support this observation. Further investigation into the mechanism of growth inhibition for *E. coli* showed that nanoparticle-bacterium interactions likely occur and that a general stress response was elicited. Extending this general approach of using well-characterized materials, multiple organisms, and measures of growth and viability to other nanomaterials will be important for understanding the interaction of nanomaterials with living systems and for interpreting the effect and eventual fate of engineered materials in the environment.

ACKNOWLEDGMENTS

We thank Tingfen Yan for assistance in generating the microarray data.

We acknowledge support from the Office of Biological and Environmental Research, U.S. Department of Energy (DOE). Oak Ridge National Laboratory is managed by UT-Battelle, LLC, for the U.S. DOE under contract no. DE-AC05-00OR22725. Ninell P. Mortensen thanks the Lundbeck Foundation for financial support.

REFERENCES

1. **Adams, L. K., D. Y. Lyon, and P. J. J. Alvarez.** 2006. Comparative ecotoxicity of nanoscale TiO_2, SiO_2, and ZnO water suspensions. Water Res. **40:**3527–3532.
2. **Asati, A., S. Santra, C. Kaittanis, S. Nath, and J. M. Perez.** 2009. Oxidase-like activity of polymer-coated cerium oxide nanoparticles. Angew. Chem. Int. Ed. **48:**2308–2312.
3. **Auffan, M., J. Rose, J. Y. Bottero, G. V. Lowry, J. P. Jolivet, and M. R. Wiesner.** 2009. Towards a definition of inorganic nanoparticles from an environmental, health and safety perspective. Nat. Nanotechnol. **4:**634–641.
4. **Barnard, A. S.** 2006. Nanohazards: knowledge is our first defence. Nat. Mater. **5:**245–248.
5. **Beliaev, A. S., D. M. Klingeman, J. A. Klappenbach, L. Wu, M. F. Romine, J. A. Tiedje, K. H. Nealson, J. K. Fredrickson, and J. Zhou.** 2005. Global transcriptome analysis of Shewanella oneidensis MR-1 exposed to different terminal electron acceptors. J. Bacteriol. **187:**7138–7145.
6. **Brayner, R., R. Ferrari-Iliou, N. Brivois, S. Djediat, M. F. Benedetti, and F. Fievet.** 2006. Toxicological impact studies based on Escherichia coli bacteria in ultrafine ZnO nanoparticles colloidal medium. Nano Lett. **6:**866–870.
7. **Brown, S. D., M. Martin, S. Deshpande, S. Seal, K. Huang, E. Alm, Y. Yang, L. Wu, T. Yan, X. Liu, A. Arkin, K. Chourey, J. Zhou, and D. K. Thompson.** 2006. Cellular response of *Shewanella oneidensis* to strontium stress. Appl. Environ. Microbiol. **72:**890–900.
8. **Brown, S. D., M. R. Thompson, N. C. VerBerkmoes, K. Chourey, M. Shah, J. Zhou, R. L. Hettich, and D. K. Thompson.** 2006. Molecular dynamics of the *Shewanella oneidensis* response to chromate stress. Mol. Cell. Proteomics **5:**1054–1071.
9. **Cotter, P. A., S. Darie, and R. P. Gunsalus.** 1992. The effect of iron limitation on expression of the aerobic and anaerobic electron transport pathway genes in *Escherichia coli*. FEMS Microbiol. Lett. **79:**227–232.
10. **De Faria, L. A., and S. Trasatti.** 1994. The point of zero charge of CeO_2. J. Colloid Interface Sci. **167:**352–357.
11. **Dumas, E. M., V. Ozenne, R. E. Mielke, and J. L. Nadeau.** 2009. Toxicity of CdTe quantum dots in bacterial strains. IEEE Trans. Nanobiosci. **8:**58–64.
12. **Farokhzad, O. C., J. J. Cheng, B. A. Teply, I. Sherifi, S. Jon, P. W. Kantoff, J. P. Richie, and R. Langer.** 2006. Targeted nanoparticle-aptamer bioconjugates for cancer chemotherapy in vivo. Proc. Natl. Acad. Sci. U. S. A. **103:**6315–6320.
13. **Gorby, Y. A., S. Yanina, J. S. McLean, K. M. Rosso, D. Moyles, A. Dohnalkova, T. J. Beveridge, I. S. Chang, B. H. Kim, K. S. Kim, D. E. Culley, S. B. Reed, M. F. Romine, D. A. Saffarini, E. A. Hill, L. Shi, D. A. Elias, D. W. Kennedy, G. Pinchuk, K. Watanabe, S. I. Ishii, B. Logan, K. H. Nealson, and J. K. Fredrickson.** 2006. Electrically conductive bacterial nanowires produced by *Shewanella oneidensis* strain MR-1 and other microorganisms. Proc. Natl. Acad. Sci. U. S. A. **103:**11358–11363.
14. **Gu, H., and M. D. Soucek.** 2007. Preparation and characterization of monodisperse cerium oxide nanoparticles in hydrocarbon solvents. Chem. Mater. **19:**1103–1110.
15. **Guzman, K. A. D., M. R. Taylor, and J. F. Banfield.** 2006. Environmental risks of nanotechnology: national nanotechnology initiative funding, 2000–2004. Environ. Sci. Technol. **40:**1401–1407.
16. **Handy, R. D., R. Owen, and E. Valsami-Jones.** 2008. The ecotoxicology of nanoparticles and nanomaterials: current status, knowledge gaps, challenges, and future needs. Ecotoxicology **17:**315–325.
17. **He, Y. T., J. M. Wan, and T. Tokunaga.** 2008. Kinetic stability of hematite nanoparticles: the effect of particle sizes. J. Nanoparticle Res. **10:**321–332.
18. **Henry, T. B., F. M. Menn, J. T. Fleming, J. Wilgus, R. N. Compton, and G. S. Sayler.** 2007. Attributing effects of aqueous C-60 nano-aggregates to tetrahydrofuran decomposition products in larval zebrafish by assessment of gene expression. Environ. Health Perspect. **115:**1059–1065.
19. **Ingram, M.** 1939. The endogenous respiration of *Bacillus cereus*. II. The effect of salts on the rate of absorption of oxygen. J. Bacteriol. **38:**613–629.
20. **Ju-Nam, Y., and J. R. Lead.** 2008. Manufactured nanoparticles: an overview of their chemistry, interactions and potential environmental implications. Sci. Total Environ. **400:**396–414.
21. **Kim, Y. S., J. H. Seo, and H. J. Cha.** 2003. Enhancement of heterologous protein expression in Escherichia coli by co-expression of nonspecific DNA-binding stress protein, Dps. Enzyme Microb. Technol. **33:**460–465.
22. **Kirchner, C., T. Liedl, S. Kudera, T. Pellegrino, A. M. Javier, H. E. Gaub, S. Stolzle, N. Fertig, and W. J. Parak.** 2005. Cytotoxicity of colloidal CdSe and CdSe/ZnS nanoparticles. Nano Lett. **5:**331–338.
23. **Klaine, S. J., P. J. J. Alvarez, G. E. Batley, T. F. Fernandes, R. D. Handy, D. Y. Lyon, S. Mahendra, M. J. McLaughlin, and J. R. Lead.** 2008. Nano-

materials in the environment: behavior, fate, bioavailability, and effects. Environ. Toxicol. Chem. **27:**1825–1851.
24. **Laberty-Robert, C., J. W. Long, E. M. Lucas, K. A. Pettigrew, R. M. Stroud, M. S. Doescher, and D. R. Rolison.** 2006. Sol-gel-derived ceria nanoarchitectures: synthesis, characterization, and electrical properties. Chem. Mater. **18:**50–58.
25. **Laberty-Robert, C., J. W. Long, K. A. Pettigrew, R. M. Stroud, and D. R. Rolison.** 2007. Ionic nanowires at 600°C: using nanoarchitecture to optimize electrical transport in nanocrystalline gadolinium-doped ceria. Adv. Mater. **19:**1734–1739.
26. **Limbach, L. K., R. Bereiter, E. Mueller, R. Krebs, R. Gaelli, and W. J. Stark.** 2008. Removal of oxide nanoparticles in a model wastewater treatment plant: influence of agglomeration and surfactants on clearing efficiency. Environ. Sci. Technol. **42:**5828–5833.
27. **Lin, W. S., Y. W. Huang, X. D. Zhou, and Y. F. Ma.** 2006. Toxicity of cerium oxide nanoparticles in human lung cancer cells. Int. J. Toxicol. **25:**451–457.
28. **Lindqvist, A., J. Membrillo-Hernańdez, R. K. Poole, and G. M. Cook.** 2000. Roles of respiratory oxidases in protecting *Escherichia coli* K12 from oxidative stress. Antonie Van Leeuwenhoek **78:**23–31.
29. **Lyon, D. Y., L. Brunet, G. W. Hinkal, M. R. Wiesner, and P. J. J. Alvarez.** 2008. Antibacterial activity of fullerene water suspensions (nC(60)) is not due to ROS-mediated damage. Nano Lett. **8:**1539–1543.
30. **Morones, J. R., J. L. Elechiguerra, A. Camacho, K. Holt, J. B. Kouri, J. T. Ramirez, and M. J. Yacaman.** 2005. The bactericidal effect of silver nanoparticles. Nanotechnology **16:**2346–2353.
31. **Murdock, R. C., L. Braydich-Stolle, A. M. Schrand, J. J. Schlager, and S. M. Hussain.** 2008. Characterization of nanomaterial dispersion in solution prior to in vitro exposure using dynamic light scattering technique. Toxicol. Sci. **101:**239–253.
32. **Nel, A., T. Xia, L. Madler, and N. Li.** 2006. Toxic potential of materials at the nanolevel. Science **311:**622–627.
33. Reference deleted.
34. **Nowack, B., and T. D. Bucheli.** 2007. Occurrence, behavior and effects of nanoparticles in the environment. Environ. Pollut. **150:**5–22.
35. **Park, B., K. Donaldson, R. Duffin, L. Tran, F. Kelly, I. Mudway, J. P. Morin, R. Guest, P. Jenkinson, Z. Samaras, M. Giannouli, H. Kouridis, and P. Martin.** 2008. Hazard and risk assessment of a nanoparticulate cerium oxide-based diesel fuel additive—a case study. Inhalation Toxicol. **20:**547–566.
36. **Park, J., K. J. An, Y. S. Hwang, J. G. Park, H. J. Noh, J. Y. Kim, J. H. Park, N. M. Hwang, and T. Hyeon.** 2004. Ultra-large-scale syntheses of monodisperse nanocrystals. Nat. Mater. **3:**891–895.
37. **Park, J. G., T. Katoh, W. M. Lee, H. Jeon, and U. Paik.** 2003. Surfactant effect on oxide-to-nitride removal selectivity of nano-abrasive ceria slurry for chemical mechanical polishing. Jpn. J. Appl. Phys. Part 1 **42:**5420–5425.
38. **Perez, J. M., A. Asati, S. Nath, and C. Kaittanis.** 2008. Synthesis of biocompatible dextran-coated nanoceria with pH-dependent antioxidant properties. Small **4:**552–556.
39. **Qi, L., Z. Xu, X. Jiang, C. Hu, and X. Zou.** 2004. Preparation and antibacterial activity of chitosan nanoparticles. Carbohydr. Res. **339:**2693–2700.
40. **Roduner, E.** 2006. Size matters: why nanomaterials are different. Chem. Soc. Rev. **35:**583–592.
41. **Ruparelia, J. P., A. K. Chatteriee, S. P. Duttagupta, and S. Mukherji.** 2008. Strain specificity in antimicrobial activity of silver and copper nanoparticles. Acta Biomater. **4:**707–716.
42. **Sahoo, S. K., and V. Labhasetwar.** 2003. Nanotech approaches to delivery and imaging drug. Drug Discov. Today **8:**1112–1120.
43. **Schubert, D., R. Dargusch, J. Raitano, and S. W. Chan.** 2006. Cerium and yttrium oxide nanoparticles are neuroprotective. Biochem. Biophys. Res. Commun. **342:**86–91.
44. **Shrivastava, S., T. Bera, A. Roy, G. Singh, P. Ramachandrarao, and D. Dash.** 2007. Characterization of enhanced antibacterial effects of novel silver nanoparticles. Nanotechnology **18:**225103.
45. **Sobek, J. M., and D. E. Talburt.** 1968. Effects of the rare earth cerium on *Escherichia coli*. J. Bacteriol. **95:**47–51.
46. **Sondi, I., and B. Salopek-Sondi.** 2004. Silver nanoparticles as antimicrobial agent: a case study on E. coli as a model for Gram-negative bacteria. J. Colloid Interface Sci. **275:**177–182.
47. **Stein, D. C., L. K. Kopec, R. E. Yasbin, and F. E. Young.** 1984. Characterization of Bacillus subtilis DSM704 and its production of 1-deoxynojirimycin. Appl. Environ. Microbiol. **48:**280–284.
48. **Stoimenov, P. K., R. L. Klinger, G. L. Marchin, and K. J. Klabunde.** 2002. Metal oxide nanoparticles as bactericidal agents. Langmuir **18:**6679–6686.
49. **Suresh, A. K., D. A. Pelletier, W. Wang, J.-W. Moon, B. Gu, N. P. Mortensen, D. P. Allison, D. C. Joy, T. J. Phelps, and M. J. Doktycz.** 2010. Silver nanocrystallites: biofabrication using Shewanella oneidensis, and an evaluation of their comparative toxicity on Gram-negative and Gram-positive bacteria. Environ. Sci. Technol. **44:**5210–5215.
49a. **Tarnuzzer, R. W., J. Colon, S. Patil, and S. Seal.** 2005. Vacancy engineered ceria nanostructures for protection from radiation-induced cellular damage. Nano Lett. **5:**2573–2577.
50. **Taylor, C. D., M. Neurock, and J. R. Scully.** 2008. First-principles investigation of the fundamental corrosion properties of a model Cu-38 nanoparticle and the (111), (113) surfaces. J. Electrochem. Soc. **155:**C407–C414.
51. **Thill, A., O. Zeyons, O. Spalla, F. Chauvat, J. Rose, M. Auffan, and A. M. Flank.** 2006. Cytotoxicity of CeO_2 nanoparticles for Escherichia coli. physico-chemical insight of the cytotoxicity mechanism. Environ. Sci. Technol. **40:**6151–6156.
52. **Van Hoecke, K., J. T. K. Quik, J. Mankiewicz-Boczek, K. A. C. De Schamphelaere, A. Elsaesser, P. Van der Meeren, C. Barnes, G. McKerr, C. V. Howard, D. Van De Meent, K. Rydzynski, K. A. Dawson, A. Salvati, A. Lesniak, I. Lynch, G. Silversmit, B. De Samber, L. Vincze, and C. R. Janssen.** 2009. Fate and effects of CeO_2 nanoparticles in aquatic ecotoxicity tests. Environ. Sci. Technol. **43:**4537–4546.
53. **Wang, W., J. Y. Howe, Y. Li, X. Qiu, D. C. Joy, M. P. Paranthaman, M. J. Doktycz, and B. Gu.** 2010. A surfactant and template free route for synthesizing ceria nanocrystals with tunable morphologies. J. Mater. Chem. **20:**7776–7781.
54. **Yang, S., K. M. Pappas, L. J. Hauser, M. L. Land, G.-L. Chen, G. B. Hurst, C. Pan, V. N. Kouvelis, M. A. Typas, D. A. Pelletier, D. M. Klingeman, Y.-J. Chang, N. F. Samatova, and S. D. Brown.** 2009. Improved genome annotation for Zymomonas mobilis. Nat. Biotechnol. **27:**893–894.
55. **Zheng, M., X. Wang, L. J. Templeton, D. R. Smulski, R. A. LaRossa, and G. Storz.** 2001. DNA microarray-mediated transcriptional profiling of the *Escherichia coli* response to hydrogen peroxide. J. Bacteriol. **183:**4562–4570.